# Inertial confinement fusion ignition criteria, critical profiles, and burn wave propagation using self-similar solutions

Cite as: Physics of Plasmas **4**, 1385 (1997); https://doi.org/10.1063/1.872314
Submitted: 19 August 1996 . Accepted: 14 January 1997 . Published Online: 04 June 1998

Roy Kishony, Eli Waxman, and Dov Shvarts

# Inertial confinement fusion ignition criteria, critical profiles, and burn wave propagation using self-similar solutions

Roy Kishony,[a),b)] Eli Waxman,[c)] and Dov Shvarts
*Physics Department, Nuclear Research Center—Negev, P.O. Box 9001, Beer-Sheva, Israel*

(Received 19 August 1996; accepted 14 January 1997)

The ignition conditions, under which a thermonuclear burn wave propagates from an initial hot spot, and the characteristics of the propagating burn wave are investigated using a set of self-similar solutions. Although the self-similar solutions exist only for external density profile that decreases as $\rho_{\rm out} \propto r^{-1}$, they are shown to provide natural ignition criteria and critical profiles for more general density profiles. The concept of working lines (WLs), attractors of trajectories in the $\rho R - T$ plane of propagating burn waves, is introduced for density profiles $\rho_{\rm out} \propto r^{-\omega}$. The WLs are found to be close and almost parallel to the ignition line (IL). The distance of the WLs from the IL is given analytically and shown to depend on all the physical processes involved. The spatial profiles of a burn wave propagating along the WLs are shown to be closely related to the self-similar critical profiles. © *1997 American Institute of Physics.* [S1070-664X(97)02604-9]

## I. INTRODUCTION

The ignition of a central hot spot in deuterium–tritium (DT) fuel, which generates a thermonuclear burn wave that propagates through the rest of the DT fuel, is crucial for achieving high gains in inertial confinement fusion (ICF).[1] Hot spot ignition and burn propagation are expected to be demonstrated in the National Ignition Facility.[1] The limited energy source ($\approx$2 MJ) is expected to provide relatively marginal hot spot ignition with relatively small areal densities,[2] hence motivating detailed investigation of the conditions under which the hot spot ignites and the burn wave propagates. The ignition conditions are often determined using simplified zero-dimensional (0-D), Widner-type models of the hot spot.[3–9] These models describe the hot spot by a few characteristic variables: The radius $R$, density $\rho$, and temperature $T$. Using these variables, one can express the energy gain and loss rates of the hot spot by the different physical mechanisms: The $\alpha$-particle transport, bremsstrahlung losses, electron heat conduction, and hydrodynamic work. The ignition line (IL) is then defined as the line in the $\rho R - T$ plane on which the energy loss and gain rates inside the hot spot are balanced.

However, the energy deposition rates, and therefore the IL, depend not only on the characteristic (averaged) variables $\rho$ and $T$, but also on the one-dimensional (1-D) spatial profiles of these variables inside the hot spot.[8,10] These profiles, called the critical profiles, are provided in the zero-dimensional (0-D) models using additional assumptions. Usually the profiles in these models are assumed to be spatially homogeneous,[3,9] or are derived by simple considerations. For example, the temperature profile can be derived by assuming a constant heat current inside the hot spot.[6]

Kirkpatrick[10] calculated the critical profiles for a small DT target filling a static spherical cavity with a constant wall temperature, assuming an isobaric and static DT. For a specified wall temperature, the equation $\dot{T}(r) \equiv \partial T(r,t)/\partial t = 0$ was iteratively solved on a discrete spatial grid. Three independent solutions were found, two of them stable and one unstable. The critical profile was defined as the unstable solution, $T_0(r_j)$, for which a positive eigenvalue of the matrix $\mathbf{M}_{ij} = \partial \dot{T}(r_i)/\partial T(r_j)|_{T=T_0}$ exists. These critical profiles, however, cannot be applied to the problem of hot spot ignition, as they do not account for the hydrodynamic expansion and for the propagation of the thermonuclear burn wave into the cold material.

In the present work a different approach for determining the ignition criteria is taken. A set of self-similar solutions, the existence of which was first pointed out by Neudachin and Sasorov,[11,12] is shown to provide both the ignition criteria and the critical profiles. Neudachin and Sasorov showed that for an outside density profile $\rho_{\rm out} = s r^{-1}$ and for $s$ higher than a certain critical value $s_{\rm cr}$, a self-similar solution that includes all the relevant physical mechanisms exists.[11,12] The critical value $s_{\rm cr}$ was used to determine the minimum $\rho R$ needed for a prolonged propagation of thermonuclear burn in density profiles that decrease similarly to $1/r$. Analytic (reducing the problem of numerically solving the partial differential equations to the much easier problem of numerically solving the self-similar ordinary differential equation) self-similar solutions were obtained for the simple case that includes only hydrodynamic and local deposition of the $\alpha$-particles, and it was shown that the distinction between stable and unstable solutions, proposed by Kirkpatrick,[10] is valid also for the set of self-similar solutions.[11] Solutions for the more general problem, including electron heat conduction, $\alpha$-particle transport and radiation losses, were obtained only by means of numerical simulations.[12] As a result, the unstable solutions, which are important for defining the ignition conditions, were not obtained for the general case.

In the present work the complete set of self-similar solutions, which includes both the stable and unstable solutions, is derived and used to define the IL for the general case where all physical processes are included. It will be shown

[a)]Electronic mail: royk@menix.bgu.ac.il
[b)]Also at: The Raymond and Beverly Sackler Faculty of Exact Science, School of Physics and Astronomy, Tel-Aviv University, Tel-Aviv, Israel.
[c)]Present address: Institute for Advance Studies, Princeton, New Jersey 08540.

that although the self-similar solutions exist only for an outside density profile that decreases as $r^{-1}$, they provide a natural global ignition condition that is applicable for more general density profiles, including the commonly studied case of constant density.

Following Kirkpatrick, we also use the unstable solutions to define the ignition criteria. However, since we are also interested in the asymptotic propagation of the burn wave after ignition, the stable solutions will also be studied and defined as part of the IL. It will be shown that after ignition the hot spot trajectories in the $\rho R-T$ plane are attracted to lines, called the working lines (WLs), which are close and almost parallel to the stable part of the IL. Thus, the stable part of the self-similar solution IL can be used as a generator for the working conditions.

The self-similar approach to the investigation of thermonuclear burn wave propagation has been previously proposed by Gus'kov, Krokhin, and Rozanov.[13] However, since the authors were not aware of the possibility of including all the relevant physical mechanisms in a single self-similar solution for the case of an $r^{-1}$ density profile, only degenerate self-similar solutions were found. Neglecting the radiation losses, including either $\alpha$-particle transport or electron heat conduction as the transport mechanism, and assuming either constant pressure or constant density inside the hot spot, four different degenerate self-similar solutions were obtained. The spatial profiles of these solutions, needed to define the coefficients of the scaling laws, were not derived in this work and were assumed to be constant. The analysis presented here shows that neither the isobaric nor the isochoric assumptions are valid in the region of the $\rho R-T$ plane where the proposed degenerate solutions exist. Therefore, the degenerate solutions of Gus'kov, Krokhin, and Rozanov do not describe self-consistently the propagation of the thermonuclear burn wave.

The main purpose of the present work is to study the relation between the recently derived complete self-similar solutions to the burn wave propagation problem, the ignition criteria, the critical profiles, and the hot spot trajectories in the $\rho R-T$ plane. The detailed derivation of the self-similar solution will be presented and discussed in a separate forthcoming publication. In the next section and in the Appendix, a description and discussion of the main properties of the complete self-similar solutions and the differences from the analytic solution of Refs. 11 and 12 is given (the explicit spatial profiles of the self-similar solutions are presented later in Sec. IV). Also introduced in Sec. II is the IL corresponding to the self-similar solutions compared with that derived from a simple 0-D model. Section III deals with the propagation of the thermonuclear burn wave after ignition. The WLs, defined as the attractors of the hot spot trajectories in the $\rho R-T$ plane after ignition, are shown to be relatively close and almost parallel to the stable part of the IL. The distance of the WLs from the IL in the $\rho R-T$ plane is given analytically in the 0-D model and shown to depend on all the physical processes involved. Section IV compares the self-similar solution profiles and the profiles of a full numerical simulation along the IL and along the WLs.

## II. THE IGNITION LINE AND THE SELF-SIMILAR SOLUTION

We shall first present the commonly used 0-D Widner-type model to describe the scaling laws of the different physical mechanisms involved. The conditions for the existence of a self-similar solution, which includes all the physical mechanisms, will be derived based on these scaling laws. Then, the self-similar IL will be constructed and compared with the IL obtained by the Widner-type model.

### A. Widner-type 0-D model

Several physical processes are involved in the thermonuclear burn propagation: Electron heat conduction, $\alpha$-particle transport, hydrodynamic motion, and radiation losses. For simplicity, in the present model local thermal equilibrium, i.e., equal electron and ion temperatures, is assumed, radiation is accounted for only by bremsstrahlung losses, and fuel depletion is neglected. Relaxing these assumptions does not change the conclusions significantly. Using the 0-D approach, the energy deposition rates inside the hot spot by the different physical mechanisms can be written as (we use the notation of Ref. 9)

$$
\begin{aligned}
&W_F=\chi_F\epsilon_\alpha V\left(\frac{\rho}{2m_i}\right)^2\langle\sigma\nu\rangle,\\
&W_\alpha=\chi_\alpha f_\alpha(\rho R,T)W_F,\\
&W_R=\chi_R A_0 V\rho^2 T^{1/2},\\
&W_W=\chi_W P\cdot SC_S,\\
&W_C=\chi_C\kappa_0 T^{5/2}\frac{T}{R}S,
\end{aligned}
\tag{1}
$$

where $W_F$ is the total fusion power produced in the hot spot, and $W_\alpha$, $W_R$, $W_W$, and $W_C$ are the energy loss rates from the hot spot by $\alpha$-particles, bremsstrahlung, hydrodynamic work and electron heat conduction, respectively. The fraction of the total $\alpha$-particles energy released in fusion reactions that escapes the hot spot, $f_\alpha$, is a function of the hot spot temperature $T$ and its areal density $\rho R$.[14] $V$ and $S$ are the hot spot volume, $4\pi R^3/3$, and area, $4\pi R^2$, respectively. The pressure inside the hot spot is $P=2C_V\rho T/3$, where $C_v=3k_B/m_i$ and the expansion velocity of the hot spot is taken to be proportional to the sound speed $C_S=(2k_BT/m_i)^{1/2}$. In general, if one wishes to study the hot spot formation stage, this velocity should be replaced with an incoming initial negative velocity,[1] which is changing according to a simple force law such as: $d(\rho V\dot{R})/dt\propto PS$. However, since in the present work we are interested in describing only the burn wave propagation stage, the assumption of expansion with sound speed velocity is satisfactory (it can easily be shown that the above force law leads to this behavior). The values of the dimensional constants $\epsilon_\alpha$, $m_i$, $A_0$, $\kappa_0$, and $k_B$ are defined similar to Refs. 1 and 9, except for the value of $\kappa_0$ which was taken from Ref. 13 and differs from that of Ref. 1 by a factor of 4 due to the different values assumed for the Coulomb logarithm ($\ln\Lambda=8$ is assumed in Ref. 13 and $\ln\Lambda=2$ is assumed in Ref. 1). Here, $\chi_F$, $\chi_\alpha$, $\chi_R$, $\chi_W$, and $\chi_C$ are dimensionless coefficients of the order of

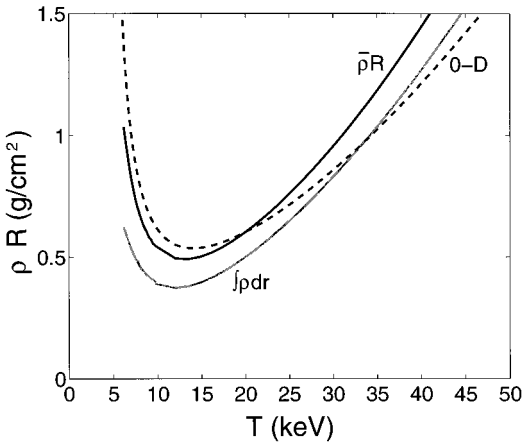


FIG. 1. The ignition line (IL) in the $\rho R-T$ plane. The 0-D IL is shown together with the self-similar IL for the mean density definition $\overline{\rho R}$ of Eq. (6b) and for the optical depth definition $\int_0^R \rho dr$ of Eq. (6a).

one, which depend on the assumed critical profiles. Assuming spatially homogeneous profiles one obtains $\chi_W=2$,[9] $\chi_F=\chi_\alpha=\chi_R=1$,[3,9] and assuming constant heat current one obtains $\chi_C=4/7$.[6]

Given the energy deposition rates inside the hot spot, Eq. (1), the IL is defined by the energy balance equation:

$$\tilde{W}_\alpha+\tilde{W}_R+\tilde{W}_W+\tilde{W}_C=1, \tag{2}$$

where $\tilde{W}_i=W_i/W_F$ is the power loss due to the $i$th process $(i=\alpha,R,W,C)$ normalized to the total fusion power. The IL, resulting from Eq. (2), is represented by the dashed line in Fig. 1.

The relative importance of the different energy loss mechanisms is shown in Fig. 2, where the normalized energy loss powers are plotted as a function of the temperature along the IL. It is seen that at low temperature, $T\leqslant 6$ keV, radiation losses are dominant, while at intermediate temperature, 6 keV$<T<$20 keV, hydrodynamic expansion losses are dominant and at high temperatures, $T>30$ keV, both hydrodynamic expansion and the $\alpha$-particle transport are important and electron heat conduction is somewhat less important. With the higher value of $\kappa_0$, assumed in Ref. 1, the relative importance of the electron heat conduction becomes larger and is about a factor of 2 higher than shown in Fig. 2. But, it is still somewhat lower than the hydrodynamic expansion and the $\alpha$-particle transport contributions.

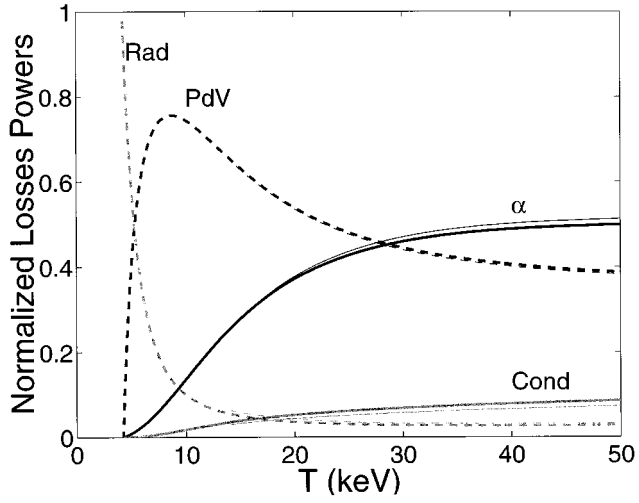


FIG. 2. Hot spot energy loss rates by the $\alpha$-particle heating $(\alpha)$, bremsstrahlung losses (Rad), electron heat conduction losses (Cond), and hydrodynamic work (PdV) as a function of the temperature along the ignition line (thick lines) and along the $\omega=0$ working line (thin lines) using the 0-D models. The partial loss rates are normalized to the total loss rate.

The convergence of $\tilde{W}_\alpha$ to a constant value at high temperatures, seen in Fig. 2, was explained in Refs. 5 and 15, as a self-regulation of the radius of the hot spot to the range of the $\alpha$-particles. A small hot spot radius relative to the $\alpha$-particle slowing down range causes a large portion of the $\alpha$-particles energy be deposited outside the spot, leading to an increased hot spot radius, which then decreases the portion of the $\alpha$-particles energy that escapes from the hot spot. This negative feedback in the $\alpha$-particles energy deposition within the hot spot, together with the fact that the time evolution of the hot spot is along trajectories that are close and parallel to the IL, as will be shown in the next section, explain the convergence of $\tilde{W}_\alpha$ to a constant value at high temperatures along the IL, seen in Fig. 2. Similar arguments hold for both the electron heat conduction and the PdV losses.

### B. 1-D self-similar solution

In order to find the critical profiles at ignition we shall now examine the conditions under which a self-similar solution to the propagating burn wave exists. These conditions were obtained by Neudachin and Sasorov,[11] but are discussed here from a different point of view based on the 0-D analysis presented in the previous section. It will also be shown that under the conditions that such a self-similar solution exists, the energy deposition rates inside the hot spot are balanced so that the profiles of that solution are indeed the critical profiles.

Self-similar solutions exist in general if no characteristic time or length exists in the problem.[16] In order to study when one can expect a self-similar thermonuclear burn wave to exist, we start by noticing that the four physical mechanisms described by Eq. (1) depend differently on the hot spot parameters, i.e., its radius $R$, density $\rho$, and temperature $T$. In order to avoid the appearance of any characteristic time or length in the solution, the ratios of the various energy loss and gain mechanisms must be time independent. Otherwise, the time, in which the importance of two such mechanism is equal, for example, would be a characteristic time. As seen from Eq. (1) the ratios between the energy loss and gain rates are functions of the hot spot temperature $T$ and areal density $\rho R$, but not of $\rho$ and $R$ independently (the weak logarithmic-dependence of the Coulomb logarithm $\ln\Lambda$ on $\rho$ and $T$ is neglected). In order not to produce new time or length scales in the problem it is necessary that the temperature and areal density scales of the self-similar solution will not vary with time:

$$T=\text{const}, \quad \rho R=\text{const}. \tag{3}$$

For a more formal derivation of these requirements see the Appendix.

Requirements (3) can only be satisfied for boundary conditions where the temperature and density outside the hot spot are given by

$$T_{\rm out}=\text{const}, \quad \rho_{\rm out}=sr^{-1}, \tag{4}$$

where $s$ is a constant having the dimensions of an areal density. Boundary conditions that are different from Eq. (4) would not allow self-similarity. For example, if $T_{\rm out}$ is not constant, the time in which $T_{\rm out}$ and $T$ become equal will serve as a characteristic time. The self-similar solution is defined by the two boundary conditions of Eq. (4), and consequently we shall deal with a two parameter family ($s$ and $T_{\rm out}$) of self-similar solutions. We shall actually see that for each pair of $s$ and $T_{\rm out}$ either no self-similar solution exists, or two solutions (stable and unstable) exist, defining the stable and unstable parts of the IL. The self-similar solution profiles for different values of $s$ are presented and discussed in Sec. IV (see Fig. 6 below).

In the above derivation we have assumed that the velocity of the material outside the hot spot is zero ($u_{\rm out}=0$). Actually, the self-similar solution also exists with any constant boundary velocity ($u_{\rm out}=$const). The constant temperature scale, defined in Eq. (3), means constant sound speed and thus, to avoid the appearance of a new time scale, all other velocities in the self-similar solution must also be constant. This implies constant boundary velocity $u_{\rm out}$ as well as constant expansion velocity $\dot{R}$.

Turning back to the ignition conditions, it should be noticed that the constant temperature requirement of Eq. (3), which was imposed by the self-similar assumptions, implies $dT/dt=0$, results in balanced energy deposition rates inside the hot spot in the self-similar solutions. Thus, the IL may be defined based on these solutions, and the spatial profiles of the solutions are critical profiles. Each of the two parameter family of self-similar solutions, $(s,T_{\rm out})$, can be mapped to a point in the $\rho R-T$ plane. Then the set of self-similar solutions with a given $T_{\rm out}$ and varied $s$ describes a line in that plane. This line is the IL for hot spots with a given outside temperature $T_{\rm out}$. When looking for solutions with $T_{\rm out}\ll 6$ keV, which is the relevant parameter range for defining an ICF IL, the IL depends only weakly on $T_{\rm out}$. Even though the self-similar IL is found by considering the case of $\rho_{\rm out}\propto r^{-1}$, it will be shown in the next sections to provide an IL for more general density profiles.

The actual mapping of the self-similar solutions profiles to the $\rho R-T$ plane can be done using various definitions for the characteristic temperature and areal density. We choose to define $T$ as the mass averaged temperature of the hot spot:

$$\overline{T}=\frac{1}{M}\int_0^R T\rho 4\pi r^2\,dr, \tag{5}$$

where $M=\int_0^R \rho 4\pi r^2\,dr$ is the total hot spot mass.

For the areal density we shall consider two definitions. The first definition is the commonly used optical depth $\overline{\rho R}$ of the hot spot:

$$\overline{\rho R}=\int_0^R \rho\,dr. \tag{6a}$$

The second definition is the product of the mean density of the hot spot and its radius, $\overline{\rho R}$, which is a natural definition for the density profile of the self-similar solutions since, from mass conservation, it can be shown to be proportional to $s$:

$$\overline{\rho R}=\left[\frac{1}{V}\int_0^R \rho 4\pi r^2\,dr\right]\cdot R=\frac{3}{2}\,s. \tag{6b}$$

Other definitions can also be used for both $T$ and $\rho R$ and there is no *a priori* superior definition, since for any of the different physical processes, different $\rho R$ and $T$ definitions are more appropriate. For example, the optical depth (6a) definition is more naturally adequate for the $\alpha$-particle transport, but the fusion rate per unit mass is better described by the mean density definition (6b). In the following we shall mainly use the $\overline{\rho R}$ definition (6b) which is more natural for the profiles of the self-similar solutions, but the more common definition of (6a) gives similar results.

The self similar ILs that correspond to the two areal densities definitions (6a) and (6b) with the mean temperature definition (5) are shown in Fig. 1 for the case $T_{\rm out}=2$ keV. ILs of other values of $T_{\rm out}$ in the relevant range $T_{\rm out}\ll 6$ keV, not shown in the figure, are very close to the $T_{\rm out}=2$ keV line at the high temperature region $T\gg T_{\rm out}$ and are slightly different at the low temperature region, where the smaller $T_{\rm out}$ is, the higher is its IL. It is seen that the two definitions of $\rho R$ result in relatively close lines. The 0-D IL is also relatively close to the self-similar ILs. Notice that this good correspondence between the 0-D IL and the self-similar IL is a consequence of the right choice of the $\chi_i$ coefficients of Eq. (1) for the 0-D model. However, this choice is only an approximation since it does not account for the different spatial distributions inside the hot spot which may change substantially at different regions of the $\rho R-T$ plane.

The self-similar IL, on the other hand, self-consistently includes the correct 1-D spatial distribution. A striking example is the hydrodynamic work term. Different descriptions for the $PdV$ term have been proposed for the 0-D models, depending on whether or not a shock wave is propagating ahead of the conduction front.[5,8,9] The self-similar solution self-consistently includes hydrodynamics and shocks together with the other physical mechanisms, and therefore naturally describes the transition between a shock wave front and a conduction front.

A self-similar thermonuclear burn wave in an outside density profile which decreases as $\rho_{\rm out}\propto r^{-1}$ exists only for values of $s$ which are higher than a certain critical value $s_{\rm cr}$. This critical value is about 0.33 g/cm$^2$ as can be deduced from Fig. 1. The value decreases to 0.23 g/cm$^2$ when local deposition of the $\alpha$-particles is assumed and decreases slightly further to 0.22 g/cm$^2$, when the bremsstrahlung radiation is also neglected. Using numerical simulations, Neudachin and Sasorov obtained $s_{\rm cr}\cong 0.43$ g/cm$^2$ for the case which includes all the physical mechanisms.[12] This value is about 25% higher than our analytic result, 0.33 g/cm$^2$. As indicated by Neudachin and Sasorov, numerical simulations

may indeed give higher values for $s_{cr}$ since the attractive region of the self-similar solution becomes very small when $s \to s_{cr}$. A similar difference of about 25%, in the critical value of $s$ between numerical simulations and analytic solutions, was obtained by Neudachin and Sasorov also for the case of local deposition of the $\alpha$-particles. In addition, the models and coefficients used by Neudachin and Sasorov to describe the various physical processes are somewhat different from those used by us, and may lead to some additional difference in the critical value of $s$.

The ILs of Fig. 1 consist of two branches that will be referred to as the left (L) and the right (R) branch. Considering the change of $\dot{T}$ as a function of $T$ we note that for fixed $\rho R$, $\dot{T}$ is zero for the two temperatures $T_L$ and $T_R$ ($T_L < T_R$) on the IL, and is positive for $T_L < T < T_R$. It follows that $\partial \dot{T}/\partial T|_{T_L} > 0$ and $\partial \dot{T}/\partial T|_{T_R} < 0$, which means that the solution at $T_L$ is unstable while the $T_R$ solution is stable. As will be shown in the next section, the fact that the right branch is stable while the left branch is unstable causes the hot spot trajectories to diverge from that left unstable branch and to be attracted to the right stable branch.

It is seen from Fig. 2 that at the left branch, where the temperature is low, the radiation losses ($\tilde{W}_R$) and the hydrodynamic work ($\tilde{W}_W$) dominate the transport and conduction mechanisms ($\tilde{W}_\alpha + \tilde{W}_C$), while at the high temperatures of the right branch the situation is reversed. Accordingly, the stable solutions of the right branch are characterized by a propagating thermonuclear burn wave in which a conduction wave, based on $\alpha$-particle transport and electron heat conduction, is moving faster and ahead of a retarded shock wave (see also the discussion of Fig. 6 below). In the unstable solutions, however, the shock wave moves ahead of the conduction wave. That picture, in which the burn wave structure changes between an unstable detonation front and a stable conduction front, could not been obtained in Refs. 11 and 12 since the set which includes both the stable and the unstable solutions was found only for the degenerate case which does not include the electron heat conduction and the $\alpha$-particle transport mechanisms and therefore always has a detonation front structure.

Kirkpatrick defined the ignition conditions by the unstable solutions of his critical profile equations. These unstable solutions correspond to the left branch of the self-similar IL. Two other, stable, solutions with temperatures above and below the temperature of the unstable solution were also found by Kirkpatrick. The stable solution with the higher temperature corresponds to the right branch of the self-similar IL. The other stable solution corresponds to a class of solution, not investigated in the present work, whose hot spot temperature is of the order of the outside temperature $T_{out}$. At high enough outside temperature the three solutions coincide and a Wheeler ignition mode occurs.[17]

If only three of the five physical mechanisms described in Eq. (1) are taken into account, the self-similar requirements, Eq. (3), and therefore the boundary conditions, Eq. (4), can be relaxed. In this case, the requirement for constant ratios between the three left $W_i$'s leads only to two equations for the three unknowns ($T$, $\rho$, and $R$) and solutions that do not satisfy the self-similar requirement (3) can be obtained. Gus'kov, Krokhin, and Rozanov[13] have proposed a self-similar solution of that kind for the propagating thermonuclear burn wave problem. Neglecting both the radiation losses ($W_R = 0$) and either the $\alpha$-particle transport ($W_\alpha = 0$) or the electron heat conduction ($W_C = 0$), only three of the five physical mechanisms described in (1) were taken into account. Thus, only two ratios of energy rates had to be kept constant. A third, non-self-similar equation was added by assuming that the hydrodynamic propagation is either much slower or much faster than the conduction front propagation. Respectively, it was assumed that either the density is constant ($\rho = \text{const}$), or that the front moves with a velocity of a shock wave $\dot{R} \propto (\rho T)^{1/2}$ and a constant pressure is assumed behind the shock ($P = \text{const}$). The three equations were then solved for the scales $T(t)$, $\rho(t)$, and $R(t)$. Although the spatial profiles of the density and pressure could be derived, they were not obtained in that work, and were rather assumed to be constant. Analyzing the various mechanisms participating in the hot spot evolution, Fig. 2, it is apparent that the radiation losses are the dominant mechanism and cannot be neglected at the low temperature region, while at the high temperature region hydrodynamics becomes important. It will also be shown that neither the assumption of constant density nor the constant pressure assumption hold at these regions. Therefore, the degenerate self-similar solutions of Gus'kov, Krokhin, and Rozanov[13] do not describe self-consistently the ignition and the burn wave propagation in any of the IL regions in the $\rho R - T$ plane. We shall return to this comparison in the next section.

## III. WORKING LINES: ATTRACTORS OF HOT SPOT TRAJECTORIES IN THE $\rho R - T$ PLANE

A simple 0-D model that is based on the energy deposition rates given in Eq. (1) is used to investigate the trajectories of hot spots in the $\rho R - T$ plane. It will be shown that after ignition the trajectories of all hot spots are attracted to lines, defined as the working lines (WLs), which will be given analytically in terms of their distance from the IL. This attraction of the hot spot trajectories to WLs, which reflects the stability of the right branch of the self-similar IL, will also be demonstrated using a full 1-D numerical simulation.

### A. 0-D model for hot spot trajectories

In the 0-D model the temperature of the hot spot changes due to the energy deposited inside the hot spot, $W_{in} = W_F - W_\alpha - W_C - W_R - W_W$. Due to the short range of the $\alpha$-particles and of the heat conducting electrons in the cold fuel outside the hot spot, the energy $W_{out} = W_\alpha + W_C$ carried by these transport mechanisms outside the hot spot is assumed to heat up a thin layer of the cold fuel outside the hot spot, from its initial temperature up to the hot spot temperature. The radiation losses $W_R$ are assumed in the present model to escape out of the entire DT pellet. The hydrodynamic work $W_W$ is assumed to decrease the hot spot internal energy as it transforms it into kinetic energy. The time evolution of the hot spot temperature $T$, mass $M = \rho \cdot V$, and radius $R$ can thus be written, similar to Refs. 8 and 15, as

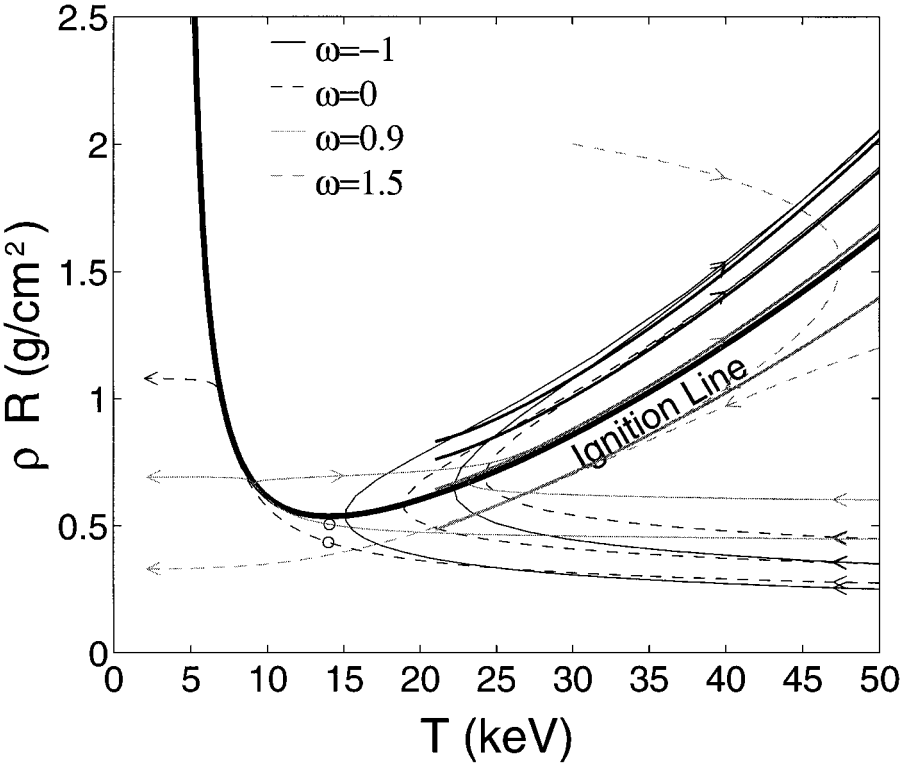


FIG. 3. The ignition line, hot spot trajectories, and working lines in the $\rho R-T$ plane as described by the 0-D model. Trajectories of hot spots with different initial conditions and with the boundary conditions $T_{\text{out}}=2$ keV and $\rho_{\text{out}}=r^{-\omega}$ for $\omega=-1$, 0, 0.9, 1.5, are shown (thin lines). Also shown are the working lines for those boundary conditions (thick lines). The marginal trajectories, which define the SCIL, are marked with ''$o$'' for $\omega=0$, 0.9.

$$
\begin{aligned}
&C_V M\dot{T}=W_{\text{in}},\\
&C_V(T-T_{\text{out}})\dot{M}=W_{\text{out}},\\
&S\rho_{\text{out}}\dot{R}=\dot{M}.
\end{aligned}
\tag{7}
$$

Since the model described by Eq. (7) takes into account the propagation of the burn wave into the initially cold fuel, the outside conditions $\rho_{\text{out}}$ and $T_{\text{out}}$, which define the mass and internal energy of the cold fuel that is overtaken by the burn wave, should be specified. Motivated by the self-similar solution, we take the conditions outside the hot spot to be $\rho_{\text{out}}=sR^{-\omega}$ and $T_{\text{out}}=$const.

The model parameters are therefore the hot spot's initial conditions for $\rho R$ and $T$ and the outside condition parameters $\omega$ and $T_{\text{out}}$. The coefficient $s$ is not a free parameter and is defined by the requirement $\rho=1/V\int_0^R sr^{-\omega}4\pi r^2\,dr$ at $t=0$.

The temporal evolution of the hot spot in the 0-D model is demonstrated in Fig. 3, presenting trajectories in the $\rho R-T$ plane for the outside conditions $\omega=-1$, 0, 0.9, 1.5, and $T_{\text{out}}=2$ keV (as pointed out before, very similar results are obtained for other outside temperatures as long as $T_{\text{out}}\ll T$). Shown in Fig. 3 are the different hot spot trajectories and the 0-D IL which is defined by Eq. (2), i.e., by $\dot{T}=0$. Note that the trajectories of all the hot spots that ignite cross the IL perpendicular to the temperature axis, i.e., with $\dot{T}=0$, regardless of their outside and initial conditions. This results from the fact that in the 0-D model the coefficients $\chi_i$ in Eq. (1) are fixed, independent of the conditions outside the hot spot. Therefore, the 0-D IL does not depend on the outside condition parameters $\omega$ and $T_{\text{out}}$ and can be viewed as a 0-D global IL. Note also that for the hot spot trajectories with $\omega>1$ the areal density $\rho R$ decreases with time as their radius $R$ increases and therefore no sustained thermonuclear burn wave can exist in a density profile that is decreasing faster than $1/r$.

As is seen from Fig. 3, ignition is possible also from points under the IL. These types of trajectories, in which the hot spot temperature initially decreases while its areal density increases, and only then the IL is crossed and the temperature starts to increase, is called sub-critical ignition.[5,7] The sub-critical ignition line (SCIL) is defined by the most marginal ignition trajectory.[5] The marginal trajectories for $\omega=0$ and for $\omega=0.9$ are shown and marked in Fig. 3. It can be seen that, unlike the IL, the SCIL does depend on the conditions outside the hot spot. Note also the divergence of the marginal trajectories near the left branch of the IL, which is in accordance with the instability of that branch discussed in Sec. II. In the present paper we focus on the IL, and the SCIL is not discussed further.

It is apparent from Fig. 3 that for any given $\omega$ all hot spot trajectories that ignite are attracted to an asymptotic trajectory. These asymptotic trajectories can be described analytically by writing the 0-D model equations (7) as a trajectory equation:

$$
\frac{dT}{d(\rho R)}=\frac{h(\rho R,T)}{\phi(\omega)},
\tag{8}
$$

where

$$h(\rho R,T)=\frac{T-T_{\rm out}}{\rho R}\cdot\frac{W_{\rm in}}{W_{\rm out}},$$

and

$$\phi(\omega)=\frac{1-\omega}{3-\omega}.$$

The variable $\rho R$ at a given temperature $T$ can be replaced with the new variable $\tau=(\rho R-H_{\rm IL})/H_{\rm IL}$, where $H_{\rm IL}$ is defined as the IL areal density for the temperature $T$ and is given by the implicit equation $h(H_{\rm IL},T)=0$. Expanding $h$ to first order about the IL point $(H_{\rm IL},T)$, $h(\rho R,T)=\tau H_{\rm IL}\partial h/\partial(\rho R)|_{\rho R=H_{\rm IL}}$, Eq. (8) can be written as

$$\tau H_{\rm IL}\frac{d\tau}{dH_{\rm IL}}=\tau_0\phi(\omega)-\tau, \tag{9}$$

where

$$\tau_0=\left(H_{\rm IL}\left.\frac{-\partial h}{\partial T}\right|_{\rho R=H_{\rm IL}}\right)^{-1}$$
$$=W_{\rm out}\left(\left.\frac{-\partial W_{\rm in}}{\partial T}\right|_{\rho R=H_{\rm IL}}(T-T_{\rm out})\right)^{-1}.$$

From Eq. (9) it follows that $\tau\to\tau_0\phi(\omega)$, provided that $\tau_0$ does not vary significantly with $H_{\rm IL}$ and that $\tau>0$ when $H_{\rm IL}$ is increasing with time or that $\tau<0$ when $H_{\rm IL}$ is decreasing (i.e., above the IL for $\omega<1$ and below the IL for $\omega>1$). Hence, for a given $T_{\rm out}$ all hot spot trajectories that ignite for $\omega<1$, or the trajectories that are below the IL for $\omega>1$, are attracted to an asymptotic trajectory, regardless of their initial conditions, which we shall call a working line (WL) for these $\omega$ and $T_{\rm out}$. The WLs are thus defined by

$$H_{\rm WL}(T,\omega)=H_{\rm IL}(T)[1+\tau_0\phi(\omega)]. \tag{10}$$

The WLs of $\omega=-1$, 0, 0.9, 1.5, and $T_{\rm out}=2$ keV are shown in Fig. 3 by the thick lines and are seen to be indeed the attractors of the corresponding hot spot trajectories for these $\omega$'s. For $\omega=1$, the self-similar solution line is both the IL and the WL.

The distance $\tau_0\phi(\omega)$ of the WLs from the IL is described in Fig. 4. The figure shows both $\tau_0$ as a function of the temperature along the stable right branch of the IL and $\phi(\omega)$ as a function of $\omega$. At the left, unstable, branch of the IL $\tau_0$ is negative. $\tau_0$, which is positive on the right branch, diverges to infinity at the minimum of the IL, while at temperatures above 25 keV $\tau_0$ is approximately given by $\tau_0\simeq0.4$.

In order to investigate the relative importance of the different physical mechanisms in determining the value of $\tau_0$, we can write $\tau_0$ [Eq. (9) assuming $T_{\rm out}\ll T$] as

$$\tau_0=\frac{\widetilde{W}_C+\widetilde{W}_\alpha}{n\widetilde{W}_\alpha+(7/2-m)\widetilde{W}_C+(1/2-m)\widetilde{W}_R+(3/2-m)\widetilde{W}_W}, \tag{11}$$

where $m=\partial\ln\langle\sigma\nu\rangle/\partial\ln T$ and $n=\partial\ln f_\alpha/\partial\ln T$.

The denominator of Eq. (11) resembles the ignition condition (2), except for the different coefficients, which result from the difference in the temperature dependence of each mechanism. Using the values for the $\widetilde{W}_i$'s given in Fig. 2, and the fact that $m$ ranges from 1 at $T\approx25$ keV to 0 at $T>50$ keV and $n\approx3/2$ over all the temperature range,[14] it can be seen that only the radiation term $(1/2-m)W_R$ can be neglected in Eq. (11). Although $\widetilde{W}_C$ is relatively small compared to $\widetilde{W}_\alpha$ and $\widetilde{W}_W$, the high 7/2 coefficient of the electron heat conduction term due to its high nonlinearity makes it comparable to the $\alpha$-particle transport and to the hydrodynamic work terms. With the higher value of $\kappa_0$, assumed in Ref. 1, the electron heat conduction becomes the dominant term in determining the distance of the WLs from the IL.

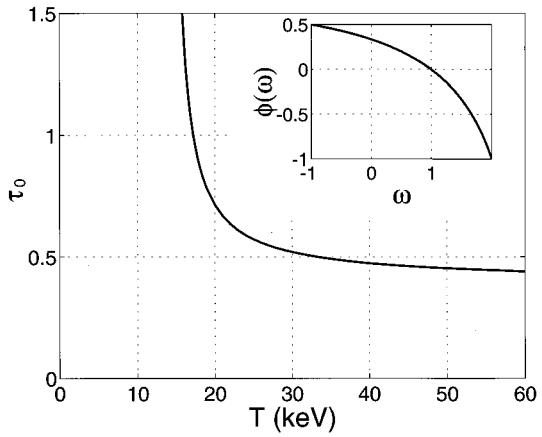


FIG. 4. The distance $\tau_0\phi(\omega)$ of the working lines from the ignition line, obtained by the 0-D model, is described. $\tau_0$ is shown as a function of the temperature along the ignition line. $\phi(\omega)$ as a function of $\omega$ is shown in the small figure.

The relative importance of the different energy loss mechanisms along the WL of the $\omega=0$ case is shown in Fig. 2. The values are seen to be very similar to those on the IL. Of course, on the WL the sum of all the energy loss mechanisms $(W_\alpha+W_R+W_W+W_C)$, by which the values in the figure are normalized, is less than the fusion power, i.e., $\widetilde{W}_\alpha+\widetilde{W}_R+\widetilde{W}_W+\widetilde{W}_C<1$ on the WL.

It should be noticed that when only two of the energy mechanisms are taken into account and assuming that they both can be approximated as power laws of the temperature, the distance $\tau_0$ becomes identically constant, i.e., the WLs are exactly parallel to the IL. This was indicated by Lindl[6] who showed that the hot spot trajectories are attracted to a line parallel to the IL when only hydrodynamic compression $(W_W\propto\rho T\dot{R}R^2)$ and electron heat conduction $(W_C\propto RT^{7/2})$ are considered. In this case from $W_W/W_C=$const one obtains a $T\propto(\rho R)^{2/5}$ trajectory.

Rozanov's[13] self-similar solution to the burn wave trajectory takes into account three mechanisms: Fusion $(W_F\propto R^3\rho^2T^m)$, hydrodynamics $(W_W\propto\rho T\dot{R}R^2)$, and either electron heat conduction $(W_C\propto RT^{7/2})$ or $\alpha$-particle transport $(f_\alpha\propto T^{3/2}/\rho R)$. Although three mechanisms are included, the solutions can still be shown to be exactly parallel to the IL, which is a consequence of the hydrodynamic term having the same scaling laws as the rate of the hot spot internal energy change $d(T\rho R^3)/dt$. The IL to which Rozanov's solutions are parallel is a degenerate IL, which is defined only by the

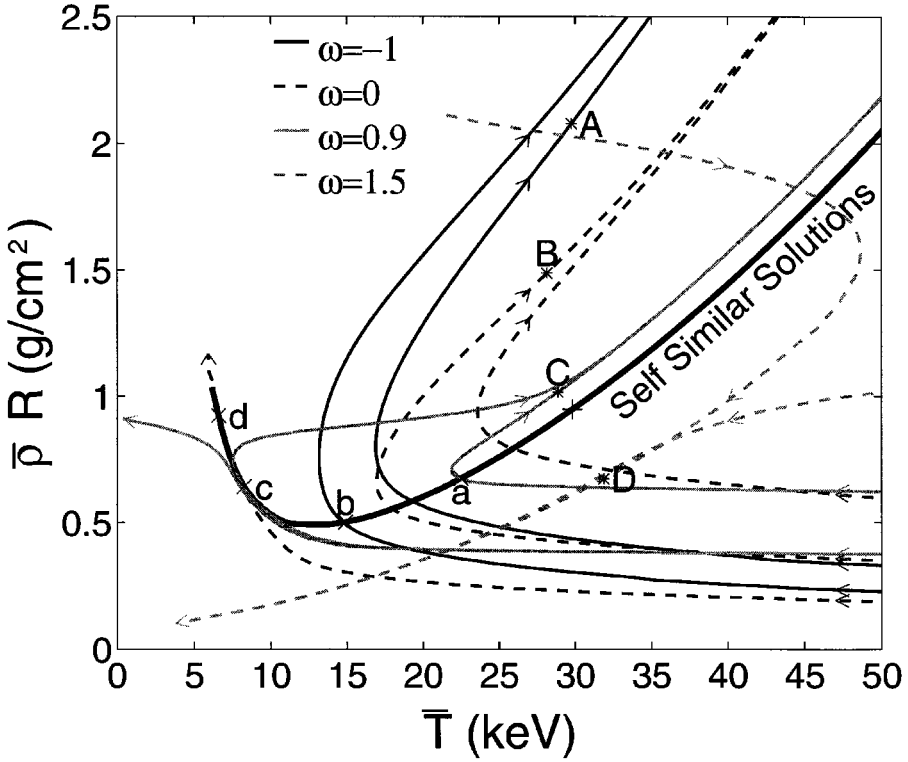


FIG. 5. The self-similar ignition line and the hot spot trajectories of a full 1-D simulation are shown in the $\overline{\rho R}-\overline{T}$ plane. The different trajectories correspond to different initial conditions and to the boundary conditions $T_{\text{out}}=2$ keV and $\rho_{\text{out}}=r^{-\omega}$ for $\omega=-1$, 0, 0.9, 1.5.

mechanisms that were taken into account and is therefore different from the nondegenerate IL that includes all the physical mechanisms. It was found, however, that the slope of this degenerate IL is close to the slope of the nondegenerate IL at high temperatures where the ratios of the various mechanisms are constant (see Fig. 2).

### B. Trajectories in a 1-D simulation

We shall now use a full 1-D numerical simulation to show that the 0-D picture of Fig. 3 remains qualitatively the same in 1-D, and that indeed the self-similar solutions line serves as the IL for the 1-D trajectories.

The simulation solves the partial differential equations given in the Appendix [Eqs. (A1)–(A3)], which include hydrodynamics, one-group diffusion of $\alpha$-particles, electron heat conduction, and bremsstrahlung losses. Equal electron and ion temperatures are assumed for simplicity and the fuel depletion is neglected.

The initial conditions used within the hot spot are of a homogeneous and static hot spot with constant temperature and density profiles. Different initial hot spot temperature and areal density are considered. The conditions outside the hot spot are taken, as in the 0-D model, to be $T_{\text{out}}=2$ keV and $\rho_{\text{out}}=r^{-\omega}$ with different $\omega$'s.

Figure 5 shows the 1-D hot spot trajectories in the $\overline{\rho R}-\overline{T}$ plane, defined by Eqs. (5) and (6b), for different initial and boundary conditions. Also shown is the self-similar IL. Qualitatively the results of the 1-D model (Fig. 5) are similar in nature to the results of the 0-D model (Fig. 3) with the self-similar solutions line as the IL. Similar to the 0-D case, the trajectories for a given $\omega$ converge to an asymptotic WL and the WLs of the different $\omega$'s converge, as $\omega\rightarrow 1$, to the self-similar IL.

This convergence of the WLs to the self-similar IL can be understood based on the asymptotic self-similar assumption. The WLs were defined to be the attractors of the hot spot trajectories in the $\rho R-T$ plane. According to the asymptotic self-similar assumption, a self-similar solution is the asymptotic solution to which all other solutions, regardless of their initial conditions, converge.[16] Thus, the self-similar solution line, described in Sec. II, is the attractor of the trajectories of the $\omega=1$ case and therefore can be thought of as the $\omega=1$ WL. The problem of finding the global IL, which is applicable for general boundary conditions, can thus be reduced to the problem of finding the WL for the $\omega=1$ case only, for which the self-similar solution exists. This conclusion is applicable when accounting for additional physical processes, such as a more complex $\alpha$-particle and radiation transport, fuel depletion, and different electron and ion temperatures. Since these processes also depend only on $T$ and $\rho R$, a self-similar solution exists for the same boundary condition. Taking into account these more complex physical processes, the right stable branch of the self-similar IL can be obtained, as was done in Ref. 12, by running a numerical simulation for the case of a hot spot propagating in a density profile with $\omega$ close to 1 ($\omega\approx 0.9$ is usually satisfactory), for which the WL is very close to the self-similar IL.

If the self-similar solution line is the IL then all hot spot's trajectories should pass this line with $\dot{\overline{T}}=0$. It is seen

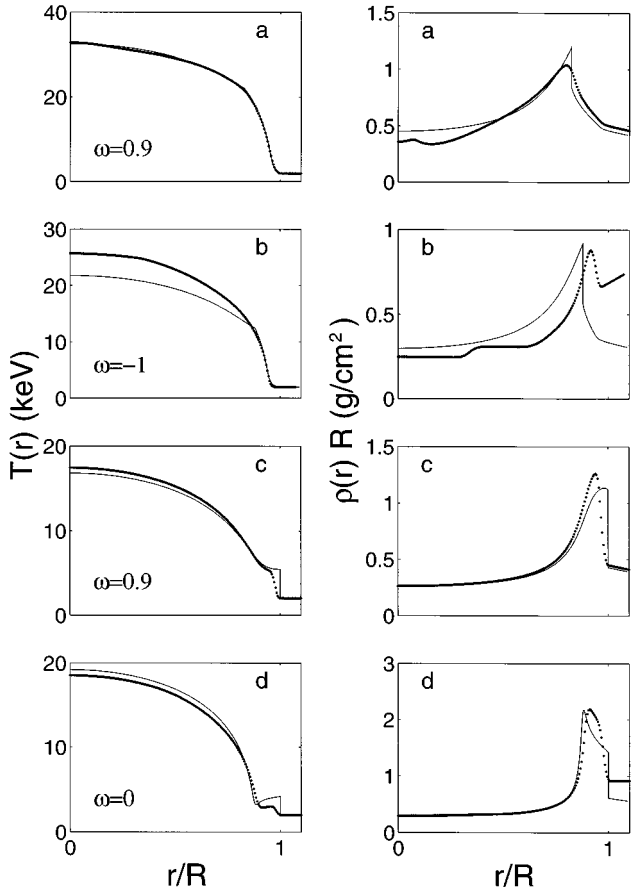


FIG. 6. The critical temperature and density (multiply by the hot spot radius, $R$) profiles at different locations on the self-similar ignition line (solid line), are compared with the profiles from full 1-D simulations at the times when the self-similar ignition line is crossed (dotted line). The four profiles correspond to the points a, b, c, and d defined in Fig. 5.

in Fig. 5 that this condition is well satisfied for $\omega$ close to 1, but for $\omega$ far from 1 it is only approximately satisfied. The fact that the IL is not crossed exactly with $\dot{\overline{T}}=0$ is a consequence of small differences in the critical profiles obtained when using $\omega$'s different from 1 (see Fig. 6), differences that do not exist in the 0-D case. Still, the most-natural definition for an IL for 1-D hot spots should be the line of the self-similar solution. This definition is independent of any assumptions regarding the initial conditions and it uses the boundary condition $\rho_{\rm out}\propto r^{-1}$, for which the WL coincides with the IL.

It can also be seen from Fig. 5 that the distance between the WLs and the IL is larger in the 1-D picture (Fig. 5) than in the 0-D picture (Fig. 3). Using the optical depth definition (6a) instead of the $\overline{\rho R}$ definition (6b), this distance become somewhat closer to that found in the 0-D picture and the deviation of the $\dot{\overline{T}}=0$ point from the IL becomes smaller. Thus, although there is no *a priori* superior definition as discussed in Sec. II B, practically the optical depth definition for the IL (see Fig. 1) should be used.

## IV. SPATIAL PROFILES

We have shown that a close relation exists between the IL and the WLs. The WLs were shown to be almost parallel to the IL and to converge to the IL as $\omega\rightarrow 1$. The relative importance of the different physical-mechanisms along the WLs was shown to be very similar to their relative importance along the IL. Motivated by this close relation between the WLs and the self-similar IL, we shall now compare their spatial profiles and show that one can learn about the profiles of the WLs from the critical profiles of the IL given by the self-similar solution. First we shall present the self-similar critical profiles, which are the solutions of the self-similar equations described in the Appendix, at different regions of the $\overline{\rho R}-T$ plane, and compare them with the profiles of the simulation at the time of ignition; then we shall compare them with the simulation profiles at the working stage.

### A. Ignition line profiles

Figure 6 compares between the hot spots profiles from simulations done with various $\omega$'s at the times where the IL is crossed and the profiles of the self-similar solution associated with the same point in the $\overline{\rho R}-T$ plane (marked by a–d in Fig. 5). As can be seen, the self-similar profiles are in very good agreement with the simulation profiles inside the hot spot $[r/R(t)<1]$ even when the outside density power $\omega$ is very far from 1. A good demonstration of the agreement between the self-similar critical profiles and the simulation profiles at ignition is the prediction of the relative position between the shock wave and the conduction front. It is seen that, as predicted by the self-similar critical profiles, the shock wave is moving behind the conduction wave in the right branch (points a and b) and is moving ahead of the conduction wave in the left branch (points c and d). Comparing the profiles of point c with those of point b, the transition between the left unstable branch and the right stable branch is seen. The profiles corresponding to the minimum value of $s$ are very similar to the self-similar profiles of point b.

### B. Working lines profiles

Although *a priori* we do not expect to find an agreement between the profiles along the WLs and the critical profiles as they correspond to different points in the $\overline{\rho R}-T$ plane, a very close relation between the profiles was found.

Figure 7 compares the profiles of the simulations of hot spots with the boundary conditions parameter $\omega=-1$, 0, 0.9, 1.5, and the self-similar critical profile with $T=30$ keV at the points marked by A–D in Fig. 5, respectively. The points were defined as the points in which the central temperature of the simulation profiles equals the central temperature of the chosen self-similar solution. The self-similar solution with $T=30$ keV was chosen only as an example; very similar results are obtained at other temperatures, $T>25$ keV, when convergence to the WLs has been achieved. The structure of a conduction wave followed by a shock wave, which characterizes the right branch of the self-similar IL, is also seen in the WL profiles. The temperature profiles of the different WLs are seen in Fig. 7 to be in good agreement with the self-similar IL profile. The main difference between the WL profiles and the self-similar profiles is in the density profiles. The density profiles of the WLs agree very well with the self-similar solution at the region behind the shock wave

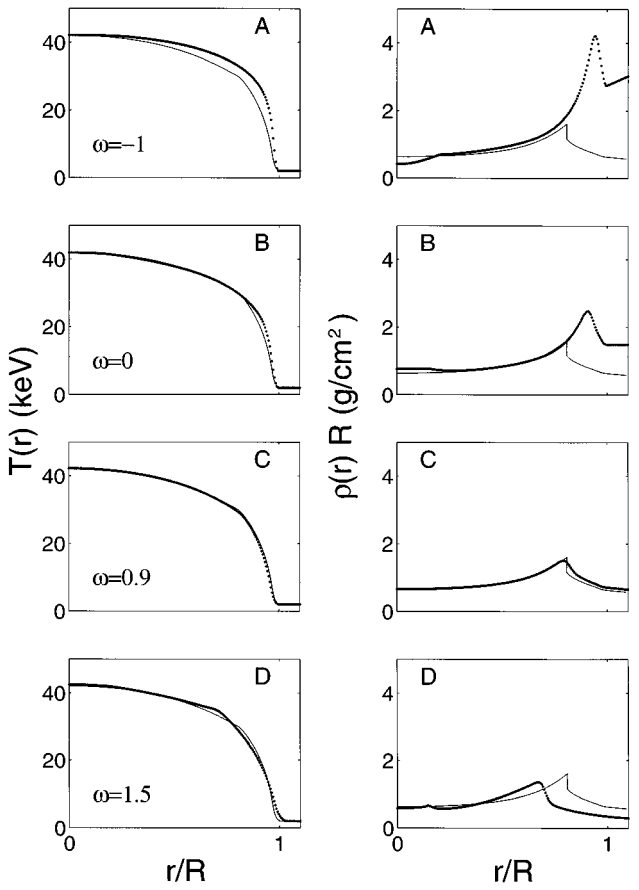


FIG. 7. The temperature and density (multiply by the hot spot radius, $R$) profiles of the self-similar ignition line at the point marked by + in Fig. 5 (solid lines) are compared with the working lines profiles (dotted lines) of $\omega=-1$, 0, 0.9, 1.5, at the points marked by A, B, C, and D in Fig. 5, when the central temperature matches the central temperature of the self-similar profile.

where the flow is supersonic and the velocity of the hydrodynamic characteristics is higher than the velocity of the self-similar expansion. Ahead of the shock wave the density profiles are defined and affected by the boundary conditions, and consequently, different profiles are observed for the different WLs. The higher $\overline{\rho R}$ of the $\omega<1$ WLs relative to the self-similar IL, which lets the temperature rise along these WLs while the temperature of the self-similar solutions stays constant, is thus mainly a consequence of a higher density ahead of the shock wave for cases A–C. For the $\omega>1$ case (D), the density ahead of the shock wave is, however, lower than the self-similar density profiles and therefore the temperature of the $\omega>1$ WLs decreases with time. It can be seen that along the WLs the isochoric and the isobaric (the pressure profile is not shown, but it is similar in nature to the density profile) assumptions used by Gus'kov, Krokhin, and Rozanov[13] are invalid.

## V. CONCLUSIONS

Hot spot ignition and the burn wave propagation conditions were investigated using a family of self-similar solutions for thermonuclear burn wave propagation. Although the physics of thermonuclear burn waves includes four different physical mechanisms, i.e., $\alpha$-particle transport, bremsstrahlung losses, electron heat conduction, and hydrodynamic-work, each with different temperature and density scalings, a self-similar solution exists provided the density profile ahead of the thermonuclear burn wave decreases as $\rho_{\text{out}}\propto r^{-1}$. The complete family of self-similar solutions, which includes both the regions of stable and unstable solutions, was obtained. Despite the required special boundary condition, it was shown that the family of self-similar solutions provides a natural definition of the ignition line (IL) and a good description of the critical profiles for hot spots with more general boundary conditions. The self-similar solutions show that the unstable part of the IL is characterized by a shock wave moving ahead of the conduction wave, while at the stable part of the IL the conduction front, driven by $\alpha$-particle transport and electron heat conduction, is running ahead of a retarded shock wave.

The self-similar solutions along the stable part of the IL were shown to also be related to the asymptotic behavior of hot spot burn waves propagating into a general outside density profile of the form $\rho_{\text{out}}\propto r^{-\omega}$. Using a simple 0-D model it was shown that for given $\omega$ the trajectories in the $\rho R-T$ plane of all the hot spots that ignite converge to a common attractor, which was called the working line (WL) of that $\omega$. The WLs were found to be parallel to the IL in most of the temperature ranges and their distance from the IL was analytically derived in terms of the relative importance of the physical mechanisms involved. This distance was shown to converge to zero as $\omega\rightarrow 1$, in accordance with the interpretation of the self-similar WL of the $\omega=1$ case as the IL. A close relation between the WLs and the self-similar IL was found to also exist for the spatial profiles. The temperature and density profiles along the different WLs agree very well with the self-similar profiles at the supersonic region behind the shock wave. The boundary conditions, defined by $\omega$, thus seem to influence only the density at the sub-sonic region between the shock and the conduction front.

Self-similar solutions of the type described in this work also exist when accounting for additional physical processes, which were not taken into account for simplicity only. For example, different electron, ion, and radiation temperatures, and a more adequate $\alpha$-particle transport can be included. Given a numerical simulation that includes these or other physical processes, the stable branch of self-similar solutions can be found easily, as was done in Ref. 12, by considering the case of a hot spot propagating in a density profile with $\omega$ close to 1 [$\omega\approx 0.9$ is usually satisfactory as can be seen from Fig. 7(C)], for which the WL is very close to the self-similar IL and provides also the self-similar profiles. The unstable solutions should be found analytically, or by running the simulation with $\omega<1$, choosing very carefully the initial conditions in order to get a marginal ignition trajectory (see the trajectories near the left branch in Fig. 5). Then, given the family of self-similar solutions, the ignition conditions, the asymptotic trajectories, and the profiles of hot spots with different boundary conditions can be constructed using the methods presented here.

The self-similar solutions can serve as the underlying 1-D solutions for analysis of the effects of two- and three-

dimensional perturbations on the ignition of hot spots and on the propagation of burn waves.


## ACKNOWLEDGMENT

We like to thank the anonymous referee for calling our attention to Refs. 11 and 12.


## APPENDIX: THE MODEL EQUATIONS AND THE DERIVATION OF THE SELF-SIMILAR SOLUTION

The hydrodynamic equations for the temperature $T(r,t)$, velocity $u(r,t)$, and density $\rho(r,t)$ of a spherical symmetric DT plasma are:

$$\frac{d\rho}{dt}+\rho\left(\frac{\partial u}{\partial r}+\frac{2u}{r}\right)=0,$$

$$\frac{du}{dt}=-\frac{1}{\rho}\frac{\partial P}{\partial r}, \tag{A1}$$

$$C_v T\rho\,\frac{d}{dt}\ln\frac{T}{\rho^{\gamma-1}}=Q,$$

where $d/dt=\partial/\partial t+u\partial/\partial r$ is the Lagrangian derivative.

An ideal gas equation of state with $\gamma=5/3$ is assumed. The pressure is thus given by $P=\frac{2}{3}C_v T\rho$, where $C_v=3k_B/m_i$.

The source term $Q$, which includes electron heat conduction, bremsstrahlung losses, and the energy deposited by the $\alpha$-particles, is given by

$$Q=\frac{1}{r^2}\frac{\partial}{\partial r}\left(r^2\kappa_0 T^{5/2}\frac{\partial T}{\partial r}\right)-A_0\rho^2 T^{1/2}+\epsilon_\alpha\Sigma\cdot n, \tag{A2}$$

where $\kappa_0=1.1\cdot10^{19}$ erg/keV$^{7/2}$ cm s, $A_0=2.8\cdot10^{23}$ cm$^5$/gr s$^3$ keV$^{1/2}$, and $\epsilon_\alpha=3.5$ MeV.

The $\alpha$-particles transport is described in the present model by a one group diffusion equation for the density $n(r,t)$ of the particles:

$$\frac{\partial n}{\partial t}=\frac{1}{r^2}\frac{\partial}{\partial r}r^2 D\,\frac{\partial n}{\partial r}-\Sigma\cdot n+S_\alpha. \tag{A3}$$

The rhs of this equation includes a diffusion term with the diffusion coefficient $D=\widetilde{D}T^{3/2}/\rho$; an absorption term (the slowing down of the $\alpha$-particles is described in the one-group model by an effective absorption) with the absorption coefficient $\Sigma=\widetilde{C}_e\rho/T^{3/2}$ where $\widetilde{C}_e$ is constant; and a source term $S_\alpha=\langle\sigma v\rangle(\rho/2m_i)^2$ where $\langle\sigma v\rangle$ is the fusion cross section. The exact dependence of $\langle\sigma v\rangle$ on the temperature is taken into account, as given in Ref. 18. The absorption of the $\alpha$-particles appears as an energy source in the last term of Eq. (A2).

If a self-similar solution to Eqs. (A1)–(A3) does exist, then all the physical quantities can be described by a separation of variable ansatz of the form:

$$\begin{aligned}
&\rho(r,t)=\rho_0(t)\cdot g(\xi),\\
&T(r,t)=T_0(t)\cdot\pi(\xi),\\
&u(r,t)=\dot{R}(t)\cdot\xi U(\xi),\\
&n(r,t)=n_0(t)\cdot\nu(\xi),
\end{aligned} \tag{A4}$$

where $\xi=r/R(t)$, and $\dot{R}=dR/dt$. $\rho_0$, $n_0$, $T_0$, and $\dot{R}$ are called the scales of the corresponding hydrodynamic variables, and $g$, $\pi$, $U$, and $\nu$ are the spatial distribution functions.

Substituting the separation of variables ansatz (A4) in the partial differential Eqs. (A1)–(A3), a set of ordinary differential equations for the spatial, $\xi$, dependence is obtained, provided that no time dependent terms are left in the equations. This requires that the following terms be time independent.

$$\alpha_1=\frac{A_0}{C_V}\frac{\rho_0 R}{T_0^{1/2}\dot{R}},\quad \alpha_2=\frac{\kappa_0}{C_V}\frac{T_0^{5/2}}{\rho_0 R\cdot\dot{R}},\quad \alpha_3=\frac{\widetilde{C}_e\epsilon_\alpha}{C_V}\frac{n_0 R}{T_0^{5/2}\dot{R}},$$

$$\alpha_4=\widetilde{D}\,\frac{T_0^{3/2}}{\rho_0 R\cdot\dot{R}},\quad \alpha_5=\frac{\langle\sigma\nu\rangle_{T_0}}{m_i^2}\frac{(\rho_0 R)^2}{n_0 R\cdot\dot{R}},$$

$$\alpha_6=\widetilde{C}_e\,\frac{\rho_0 R}{T_0^{3/2}\cdot\dot{R}},\quad \alpha_7=\frac{\dot{R}^2}{c_0^2},$$

where $c_0^2=\frac{2}{3}C_V T_0$. An additional requirement is $\dot{X}R/X\dot{R}=$const, where $X$ stands for the hydrodynamic scales $\rho_0$, $n_0$, $T_0$, and $\dot{R}$. The existence of a solution (beside the trivial constant solution) for these equations is not *a priori* guaranteed since the number of conditions to be satisfied is larger than the number of variables. Notice that the $\alpha_i$ terms depend on $\rho_0$, $n_0$, and $R$ only through the terms $\rho_0 R$ and $n_0 R$; it is found that one nontrivial solution does exist:

$$\rho_0 R=\text{const},\quad n_0 R=\text{const},\quad T_0=\text{const},\quad \dot{R}=\text{const}. \tag{A5}$$

The spatial profiles of the self-similar solution are then derived by numerically integrating the ordinary differential equations for the spatial distribution functions $g(\xi)$, $\pi(\xi)$, $U(\xi)$, and $\nu(\xi)$ with the appropriate boundary conditions. These ordinary differential equations can be shown to have a singularity on the line $U+C=1$, where $U$ is defined by Eq. (A4) and $C$ is defined similarly by:

$$c=\dot{R}\cdot\xi C(\xi)\quad\text{where}\quad c=\left(\frac{\partial P}{\partial\rho}\right)_T^{1/2}=\frac{2}{3}C_V T.$$

It should be noticed here that the singularity line is determined by the sound velocity in constant temperature and not the adiabatic sound velocity that was shown to determine the singularity line of the Neudachin and Sasorov self-similar solution.[11,12] This difference arises from the fact that the solution of Neudachin and Sasorov does not include any conduction mechanisms which tend to keep a smooth temperature profile. The line $U+C=1$, called the sonic line, describes the points where small perturbations travel with the same velocity as the profile stretch velocity $\xi\dot{R}$ at the same point. A point $\xi_0$ that is under the sonic line $(U(\xi_0)+C(\xi_0)<1)$ cannot hydrodynamically influence the conditions at $\xi>\xi_0$.

It can be shown that the boundary conditions imply that the self-similar solution is above the sonic line at $\xi=0$ and is under the sonic line at $\xi=1$. Hence, the self-similar solution must cross the sonic line. This cross of the sonic line is done at the discontinuity of the shock wave and thus the self-similar solutions are supersonic behind the shock and are

sub-sonic ahead of it. The position $\xi_s$ of the shock is determined by the boundary conditions and, as shown in the text, for given boundary conditions, there exist two solutions—the left branch solution in which $\xi_s=1$ and the right branch solution in which $\xi_s<1$. In the Neudachin and Sasorov analytic solution, however, there were no conduction mechanisms and therefore the front was always lead by a shock ($\xi_s=1$).


[1]J. D. Lindl, Phys. Plasmas **2**, 3933 (1995).
[2]S. W. Haan, S. M. Pollaine, J. D. Lindl, L. J. Suter, R. L. Berger, L. V. Powers, W. E. Alley, P. A. Amendt, J. A. Futterman, W. K. Levedahl, M. D. Rosen, D. P. Rowley, R. A. Sacks, A. I. Shestakov, G. L. Strobel, M. Tabak, S. V. Weber, G. B. Zimmerman, W. J. Krauser, D. C. Wilson, S. V. Coggeshall, D. B. Harris, N. M. Hoffman, and B. H. Wilde, Phys. Plasmas **2**, 2480 (1995).
[3]See National Technical Information Service Document No. SAND792454 (M. W. Widner, ''Fuel energy balance studies of pellet ignition requirements,'' Sandia National Laboratories, SAND-79-2454). Copies may be ordered from the National Technical Information Service, Springfield, Virginia 22161.
[4]R. C. Kirkpatrick, Nucl. Fusion **19**, 69 (1979).
[5]S. Atzeni and A. Caruso, Nuovo Cimento B **80**, 71 (1984).
[6]J. D. Lindl, *International School of Plasma Physics Piero Caldirola: Inertial Confinement Fusion*, edited by A. Caruso and E. Sindoni (Editrice Compositori, Bologna, Italy, 1988), pp. 617–631.
[7]M. M. Basko, Nucl. Fusion **30**, 2443 (1990).
[8]O. B. Vygovskii, S. Yu. Gos'kov, D. V. Il'in, A. A. Levkovskii, V. B. Rozanov, and V. E. Sherman, ''Criterion of formation of a thermonuclear burn wave in deuterium–tritium targets,'' translated from a preprint (manuscript) of the Lebedev Physics Institute (Plenum, Moscow, 1993), p. 85.
[9]V. B. Rozanov, C. P. Verdon, M. Decroisette, S. Yu. Gus'kov, J. D. Lindl, K. Nishihara, and H. Takabe, in *Energy from Inertial Fusion*, edited by W. J. Hogan (International Atomic Energy Agency, Vienna, 1995), p. 56.
[10]R. C. Kirkpatrick, Nucl. Fusion **21**, 1457 (1981).
[11]V. V. Neudachin and P. V. Sasorov, Sov. J. Plasma Phys. **14**, 567 (1988).
[12]V. V. Neudachin and P. V. Sasorov, Nucl. Fusion **33**, 475 (1993).
[13]S. Yu. Gus'kov, O. N. Krokhin, and V. B. Rozanov, Nucl. Fusion **16**, 957 (1976).
[14]O. N. Krokhin and V. B. Rozanov, Sov. J. Quant. Electron **2**, 393 (1973).
[15]A. Birenboim, E. Greenspan, and D. Shvarts, Nucl. Fusion **19**, 1605 (1979).
[16]Ya. B. Zel'dovich and Yu. P. Raizer, *Physics of Shock Waves and High Temperature Hydrodynamic Phenomena* (Academic, New York, 1968), Chap. XII.
[17]R. C. Kirkpatrick and J. A. Wheeler, Nucl. Fusion **21**, 389 (1981).
[18]L. M. Hively, Nucl. Fusion **17**, 873 (1977).